Off-energy-shell behavior of the T matrix for realistic local N-N potentials with soft or hard cores

J. L. Ballot, M. L'Huillier, and P. Benoist-Gueutal
Institut de Physique Nucléaire, Division de Physique Théorique, 91406 Orsay, France*
(Received 21 April 1975)

Off-energy-shell T matrix elements for any partial wave are calculated using realistic local two-nucleon potentials with soft or hard cores. The off-shell behaviors are discussed in relation to on-shell values. Off-shell cross sections involved in the impulse approximation of nuclear reactions are analyzed. The validity of some usual on-shell approximations is examined.

[NUCLEAR REACTION Calculated off-energy-shell T matrix for local realistic potential with soft or hard cores.]

I. INTRODUCTION

Our present knowledge of nuclear forces comes mainly from the analysis of two-nucleon scattering data at laboratory energies up to 400 MeV.[1-2] This information determines only the on-the-energy-shell nucleon-nucleon T matrix elements which can be accounted for accurately in terms of a great number of potential models such as local potentials with soft cores,[3-7] local potentials with hard cores,[5-8,9] and separable potentials.[10-13]

Despite the fact that these realistic potentials are not strictly equivalent in reproducing two-nucleon scattering data, as reflected in Fig. 1, there is no fundamental criterion to favor or discard a particular one of them. However, their off-the-energy-shell behaviors might *a priori* be different. The off-shell properties of the N-N force are involved in many problems where the two-body interaction takes place in the presence of a third or more particles. Thus, many-body calculations could be a tool for selecting between equivalent on-shell two-nucleon interactions. Many papers have been devoted to this purpose in the three-body problems such as electron deuteron breakup, deuteron photodisintegration, p-p bremsstrahlung, three-body bound and scattering states, etc..... But up to now several reasons prevented one from drawing clear-cut conclusions. One of these reasons is that the various many-body data are not equally sensitive to the two-body off-energy-shell effects, another is the consequence of necessary approximations made to solve many-body problems; moreover, recent studies in ^{3}He and ^{3}H bound states conjecture three-body forces.[14]

Our purpose is to study the sensitivity of proton-deuteron breakup reactions in the range of a few hundred MeV to two-nucleon off-shell effects. This will be analyzed in a forthcoming paper. The preliminary work, which is the object of the present paper, consists in the calculation and analysis of the off-energy-shell T matrix elements for several realistic potentials.

Srivastava and Sprung[15] pioneered in this domain by proposing a practical method of computing off-energy-shell T matrix elements for local spin-dependent potentials with soft or hard cores. They

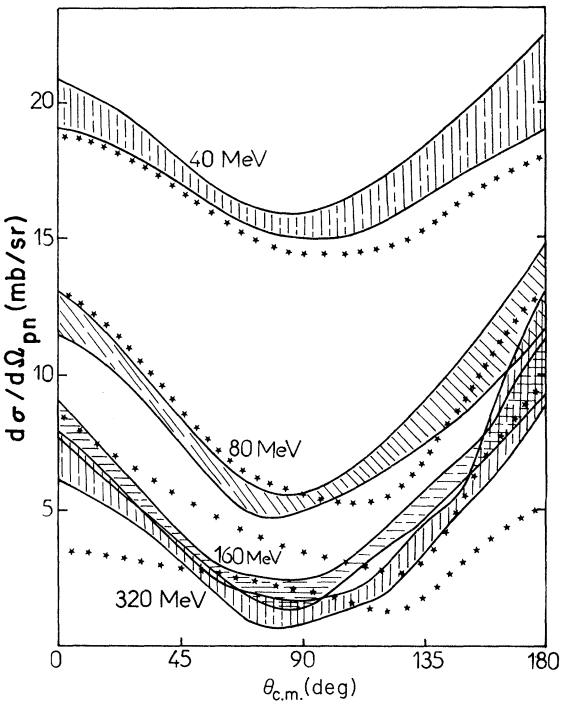

FIG. 1. p-n differential cross sections in the center-of-mass system at 40, 80, 160, and 320 MeV laboratory energies. The starred curves correspond to the Tabakin potential, the shaded domains indicate the spreading of the results for the HJ, RHC, RSC, SSO, and G1 local potentials.

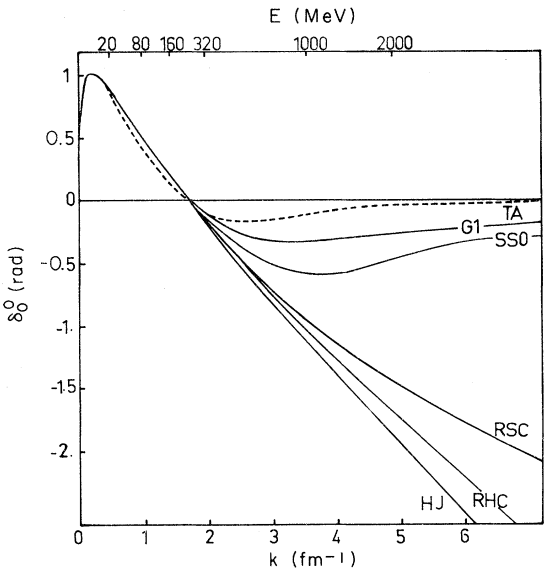

FIG. 2. $^1S_0$ phase shift plotted against k (and $E = 2\hbar^2k^2/m$ on the upper scale) for five local potentials and Tabakin's interaction.

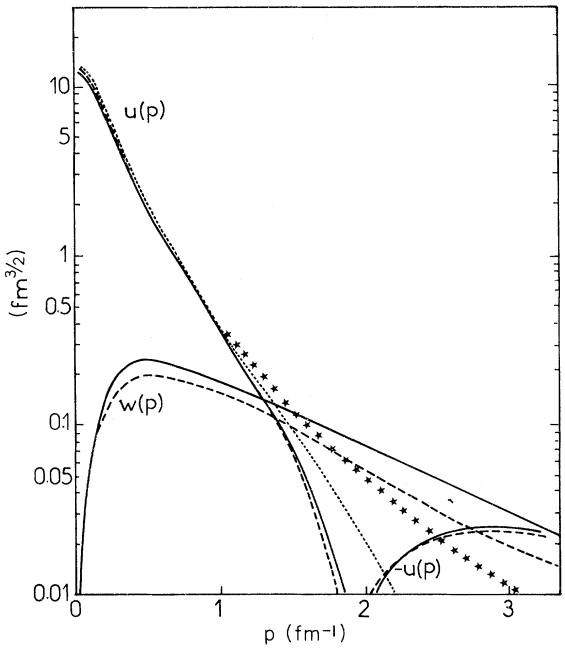

FIG. 4. $S(u(p))$ and $D(w(p))$ components of the deuteron wave function in momentum space for (HJ) (solid line) and (SSO) (dashed line) potentials. Hülthen (starry line) and Moravscik (dotted line) S-wave functions are drawn for comparison.

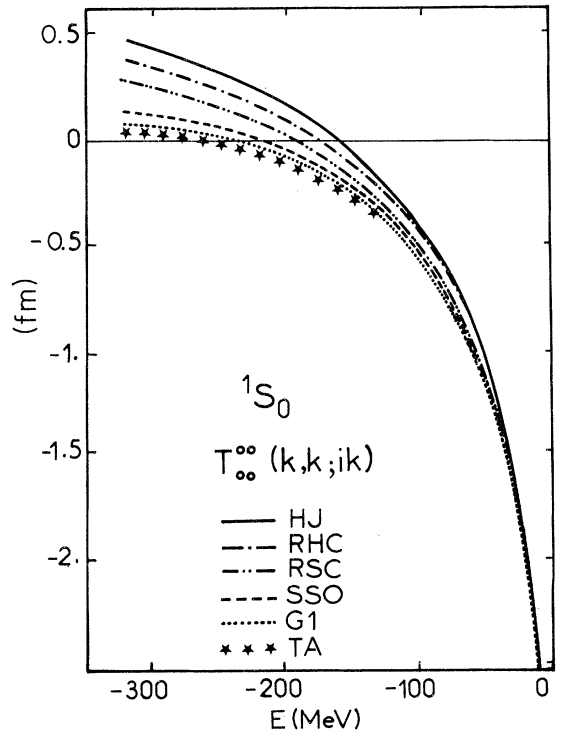

FIG. 3. $^1S_0$ matrix elements $T^{00}_{00}(k,k;ik)$ at negative energies plotted against $E = -2\hbar^2k^2/m$.

also studied the off-shell behavior of a class of phase-equivalent $^1S_0$ separable and local potentials. Several authors[16-18] have handled the $^1S_0$, $^3S_1$, or P partial amplitudes for different realistic classes of local, separable, or momentum dependent interactions. Nevertheless, as far as we know, only a few studies have been devoted to $l > 0$ off-energy-shell amplitudes with realistic potentials. Takemiya[18] has given some examples for

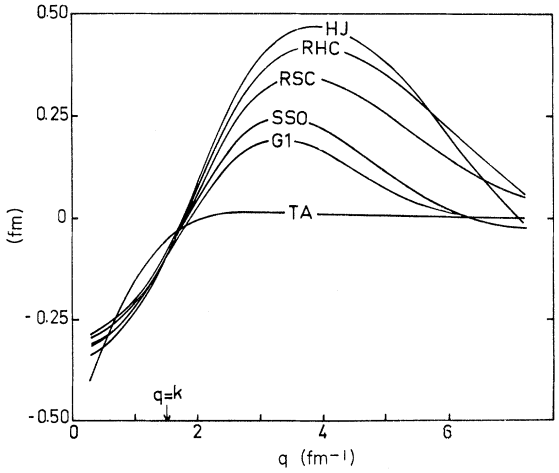

FIG. 5. $^1S_0$ half-off-shell matrix elements $e^{-i\delta_0^0(k)} \times T^{00}_{00}(q,k;k)$ in fm at $k = 1.5$ ($E = 186$ MeV lab).

Hamada-Johnston potential at fixed 150 MeV laboratory energy and fully off shell. McCarthy and Tandy,[19] studying $^2H(p,2p)n$ reaction, have computed half-shell T matrix elements involved in the off-shell spectator approximation at incident energies from 14.4 MeV up to 100 MeV. Stephenson *et al.*[20] have calculated the p-p cross sections relevant to a factorized impulse approximation treatment of $(p,2p)$ reactions on heavy nuclei from 150 MeV up to 350 MeV in the energy sharing geometry for Hamada-Johnston, Bryan-Scott, and Reid's potentials (without Coulomb forces).

In Sec. II, we recall the basic equations and comment briefly on the numerical method. In Sec. III, we analyze the results on the energy shell at positive and negative energy in order to classify them with respect to some main features of the potentials such as the high energy phase shift assumptions, the smoothness or the hardness of the core. In Sec. IV, we present for each partial wave half-shell and fully off-shell results and analyze to what extent they are correlated to on-shell input. In Sec. V, we calculate off-shell cross sections which appear in the impulse approximation and examine the validity of some on-shell approximations. In Sec. VI we give our conclusions. More details may be found in L'Huillier's thesis.[21]

II. FORMALISM

A. Basic equations for two-body T-matrix elements and conventions

We define the two-body $T(z)$ operator, function of the complex energy z, by

$$T(z) = V + V(z - H_0)^{-1}T(z)\,, \tag{1}$$

where H_0 is the kinetic energy operator and V the Hermitian potential operator.

Let us define the Møller operator $\Omega(z)$ by

$$T(z) = V\Omega(z)\,; \tag{2}$$

it satisfies the integral equation

$$\Omega(z) = 1 + (z - H_0)^{-1}V\Omega(z)\,, \tag{3}$$

which reads

$$(z - H_0 - V)\Omega(z) = z - H_0\,. \tag{4}$$

We assume the potential V to be a short range static local interaction with a soft or a hard core. We neglect the neutron-proton mass difference and denote by m the nucleon mass. Then we define the relative momentum x by

$$\overline{E} = \frac{\hbar^2}{m}x^2 \quad \text{with} \quad \begin{cases} x = k \geq 0 & \text{for } \overline{E} \geq 0\,, \\ x = ik,\ k > 0 & \text{for } \overline{E} < 0\,, \end{cases} \tag{5}$$

E and $\overline{E} = E/2$ being the two-nucleon laboratory and center of mass energies, respectively.

The Møller operator $\Omega^+(\overline{E} + i\epsilon)$ satisfies an inhomogeneous equation which reads in a mixed representation

$$\langle \vec{r} \,|\, (\overline{E} - H_0 - V)\Omega^+(\overline{E} + i\epsilon) \,|\, \vec{p} \rangle = (\overline{E} - (\hbar^2/m)p^2)\langle \vec{r} \,|\, \vec{p} \rangle\,, \tag{6}$$

with the asymptotic conditions given by Eq. (3). The plane wave is normalized as follows:

$$\langle \vec{r} \,|\, \vec{p} \rangle = (2\pi)^{-3/2} \exp(i\vec{p} \cdot \vec{r})\,. \tag{7}$$

In order to obtain the off-shell matrix elements in momentum representation,

$$T(\vec{q}, \vec{p}; x) = \langle \vec{q} \,|\, T(x) \,|\, \vec{p} \rangle\,, \tag{8}$$

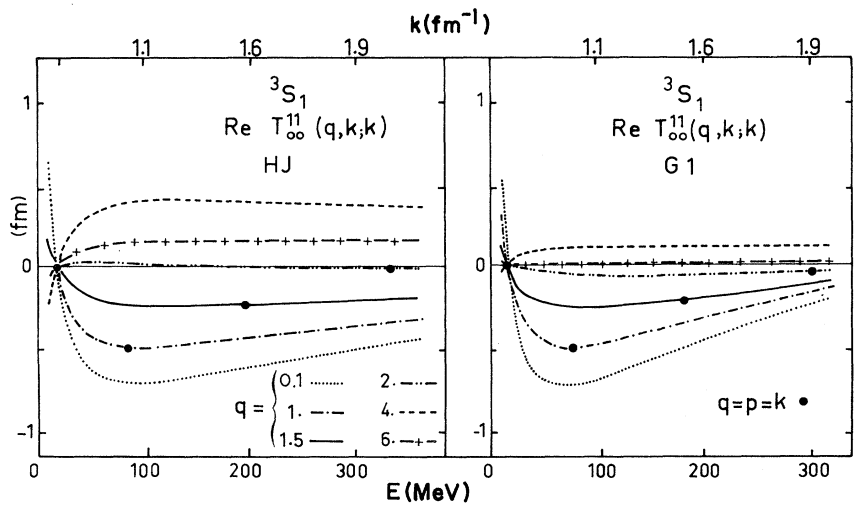

FIG. 6. Half-off-shell $\mathrm{Re}\,T_{00}^{11}(q,k;k)$ in fm for HJ and G1 forces. The lines correspond to different q momenta. The dots locate the on-shell values.

we calculate the wave function

$$\langle \vec{r} \,|\, \Psi_{\vec{p}} \rangle = \Psi(\vec{r} \,|\, \vec{p}; x) = \lim_{\epsilon \to 0^+} \langle \vec{r} \,|\, \Omega^+(E + i\epsilon) \,|\, \vec{p} \rangle \tag{9}$$

by solving Eq. (6). Then we perform the quadrature

$$T(\vec{q}, \vec{p}; x) = \langle \vec{q} \,|\, V \,|\, \Psi_{\vec{p}} \rangle \,. \tag{10}$$

We expand the wave function $\Psi(\vec{r} \,|\, \vec{p}; x)$ and the scattering amplitude $T(\vec{q}, \vec{p}; x)$ in the angular momentum representation (LSJM):

$$\Psi^S_{\sigma',\sigma}(\vec{r} \,|\, \vec{p}; x) = \sum_{JLL'} (2/\pi)^{1/2} i^L U^{JS}_{L'L}(r \,|\, p; x) D^{JS}_{L'\sigma' L\sigma}(\hat{r}, \hat{p}) \,, \tag{11}$$

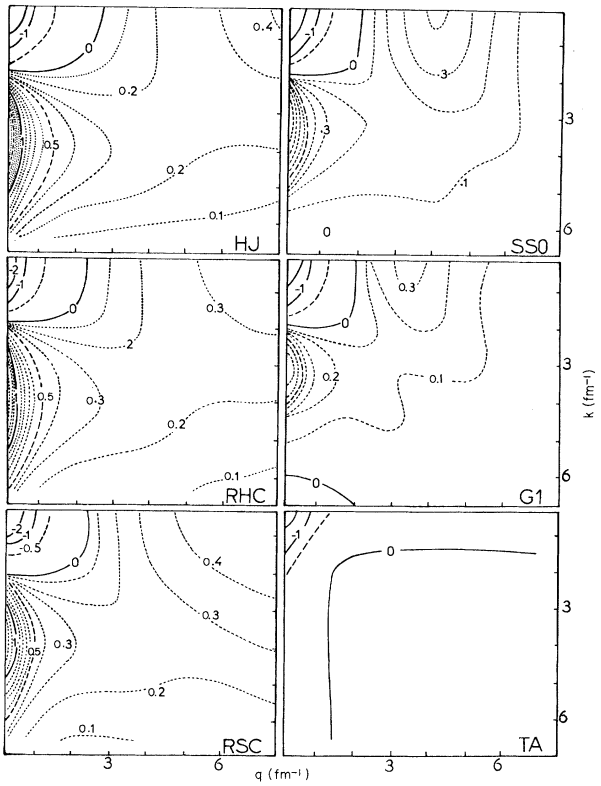

FIG. 7. $^1S_0$ half-shell isoamplitudes $e^{-i\delta_0^0(k)} \times T^{00}_{00}(q, k; k)$ at positive energies. The solid lines are the integer values of the isoamplitudes in fm, the dashed ones are the half integer values and the dotted lines are relative to a mesh of 0.1 fm. Note that the on-shell values are plotted along the diagonal; this line cuts the isocurves at fairly similar values for all potentials when k is smaller than 2 fm^{-1}. This is relevant to the good fitting of the $^1S_0$ phase shift by all the interactions. Upwards of 2 fm^{-1} the amplitudes are functions of the hardness of the core potential.

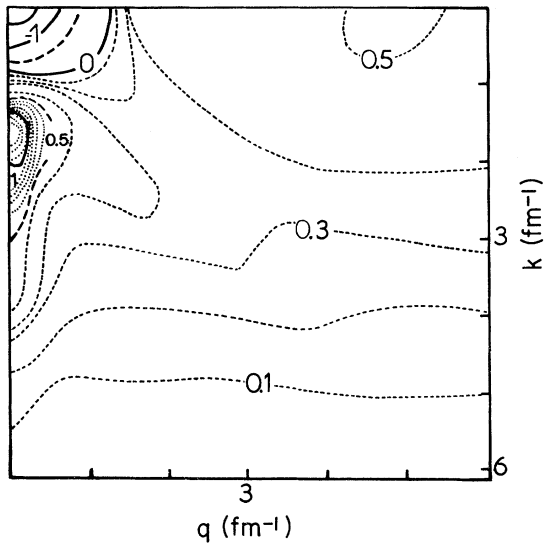

FIG. 8. $^1S_0$ half-shell isoamplitudes $e^{-i\delta_0^0(k)} T^{00}_{00}(q, k; k)$ in fm for a square well $a = 2.54$ fm, $V_0 = 14.5$ MeV.

$$T^S_{\sigma',\sigma}(\vec{q}, \vec{p}, x) = \frac{2\hbar^2}{\pi m} \sum_{JL'L} i^{L-L'} T^{JS}_{L'L}(q, p; x) D^{JS}_{L'\sigma' L\sigma}(\hat{q}, \hat{p}) \,, \tag{12}$$

$$D^{JS}_{L'\sigma' L\sigma}(\hat{q}, \hat{p}) = \sum_{Mmm'} Y^{m'}_{L'}(\hat{q}) Y^{m*}_{L}(\hat{p}) (2J+1) \times \begin{pmatrix} L' & S & J \\ m' & \sigma' & -M \end{pmatrix} \begin{pmatrix} L & S & J \\ m & \sigma & -M \end{pmatrix} , \tag{13}$$

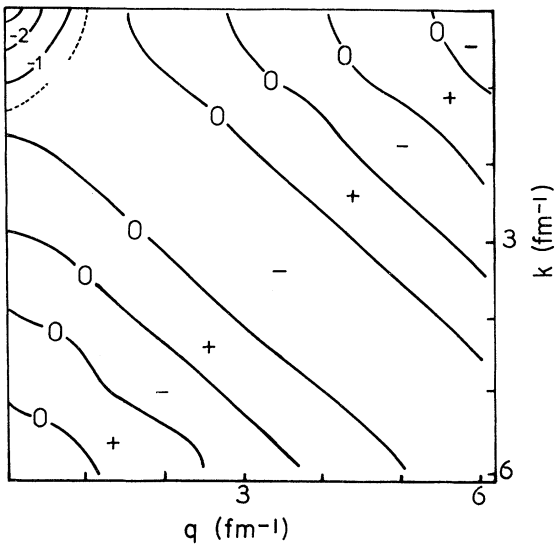

FIG. 9. $^1S_0$ half-shell isoamplitudes $e^{-i\delta_0^0(k)} T^{00}_{00}(q, k; k)$ for the same square well as in Fig. 8 but with a hard core of $r_c = 0.5$ fm.

$\hat{q}$ and $\hat{p}$ representing the angular part of the vectors $\vec{q}$ and $\vec{p}$, respectively. The wave function $U^{JS}_{L'L}(r|p;x)$ satisfies a coupled second order inhomogeneous differential system of equations which reads, in case of a local interaction with a hard core for $r \leq r_c$,

$$\left[\frac{d^2}{dr^2}+x^2-\frac{L'(L'+1)}{r^2}\right]\theta(r-r_c)rU^{JS}_{L'L}(r|p;x)-\frac{m}{\hbar^2}\sum_{\Lambda}V^{JS}_{L'\Lambda}(r)\theta(r-r_c)rU^{JS}_{\Lambda L}(r|p;x)$$
$$-\delta(r-r_c)\frac{d}{dr}[rU^{JS}_{L'L}(r|p;x)]+(x^2-p^2)\delta_{L'L}\theta(r_c-r)rj_L(pr)=(x^2-p^2)\delta_{L'L}rj_L(pr)\,, \tag{14}$$

$\theta(r-r_c)$ and $\delta(r-r_c)$ denoting the usual Heaviside and Dirac distributions. The solution $U^{JS}_{L'L}(r|p;x)$ vanishes at the origin or inside a hard core and behaves at large r as

$$prU^{JS}_{L'L}(r|p;x)\xrightarrow[r\to\infty]{}\delta_{L'L}\sin(pr-\tfrac{1}{2}L\pi)-p(-i)^{L'}T^{JS}_{L'L}(x,p;x)e^{ixr}\,. \tag{15}$$

The coefficients $T^{JS}_{L'L}(x,p;x)$ are the half-shell amplitudes at energy $\bar{E}$. For $x=p$ they reduce to the on-shell amplitudes which are related to the phase shifts (note that we do not consider the Coulomb case). The prescription Im $x>0$ implies an outgoing wave behavior in case of positive energy $\bar{E}$ and an exponential decay if $\bar{E}$ is negative. In Eq. (14) $V^{JS}_{L'L}(r)$ is the local real interaction in the $(LSJM)$ representation:

$$\langle\vec{r}'s\sigma'|V|\vec{r}s\sigma\rangle=\frac{\hbar^2}{m}\sum_{JL'L}D^{JS}_{L'\sigma'L\sigma}(\hat{r}',\hat{r})\delta(r-r')V^{JS}_{L'L}(r)\,. \tag{16}$$

Then the T matrix amplitudes are obtained from the equation

$$T^{JS}_{L'L}(q,p;x)=\tau^{JS}_{L'L}(q,p;x)+\sum_{\Lambda}\int_{r_c}^{\infty}\left[j_{L'}(qr)-j_{L'}(qr_c)\frac{h^{(-)}_{L'}(xr)}{h^{(-)}_{L'}(xr_c)}\right]\frac{m}{\hbar^2}V^{JS}_{L'\Lambda}(r)U^{JS}_{\Lambda L}(r|p;x)r^2\,dr\,, \tag{17}$$

$\tau^{JS}_{L'L}$ represents the T matrix amplitude corresponding to scattering on a hard sphere of radius r_c.

$$\tau^{JS}_{L'L}(q,p;x)=\delta_{L'L}\left\{\frac{r_c}{p^2-q^2}\left[(p^2-x^2)j_L(pr_c)qr_cj'_L(qr_c)\right.\right.$$
$$\left.\left.-(q^2-x^2)j_L(qr_c)pr_cj'_L(pr_c)\right]-r_cj_L(pr_c)j'_L(qr_c)xr_c\frac{h'^{(+)}_L(xr_c)}{h^{(+)}_L(xr_c)}\right\}\,, \tag{18}$$

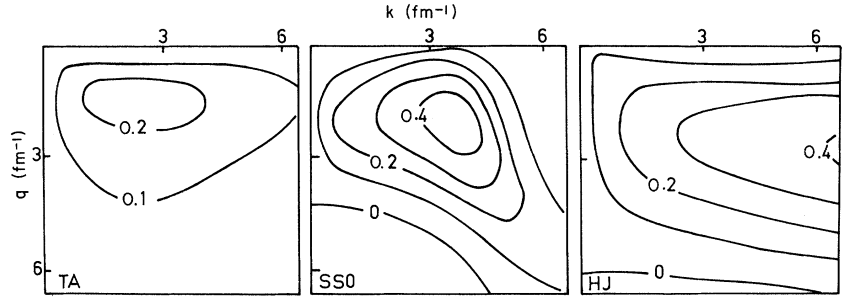

FIG. 10. $^1P_1$ half-shell isoamplitudes $e^{-i\delta^1_1(k)}T^{10}_{11}(q,k;k)$ in fm.

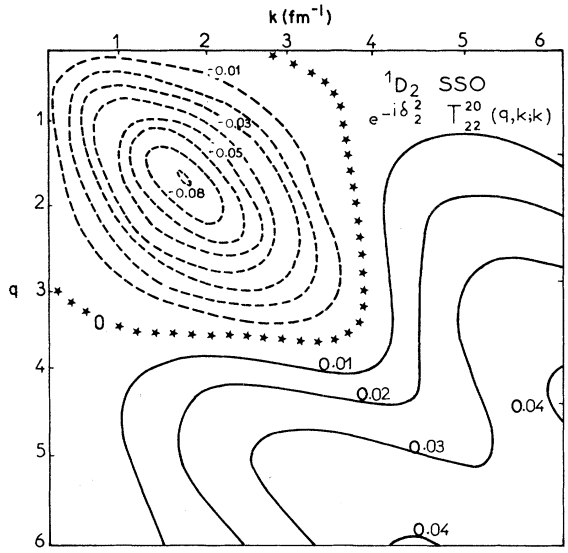

FIG. 11. $^1D_2$ half-shell isoamplitudes $e^{-i\,\delta_2^2(k)}T_{22}^{20}(q,k;k)$ in fm.

where $j_L'(\rho)$ and $h_L'^{(+)}(\rho)$ stand, respectively, for the first derivative of the Bessel function $j_L(\rho)$ and a first-kind Hankel function $h_L^{(+)}(\rho)$. The derivation of the half-off-energy shell amplitude is straightforward:

$$\tau_{L'L}^{JS}(q,k;k) = -\frac{1}{k}\frac{j_L(qr_c)}{h_L^{(+)}(kr_c)}, \tag{19}$$

and for the phase shifts we obtain

$$\delta_L(k) = -\arctan\frac{j_L(kr_c)}{n_L(kr_c)}. \tag{20}$$

For large k values, the phase shift goes to infinity as $-(kr_c - \frac{1}{2}L\pi)$, and $\tau_{L'L}^{JS}$ has an oscillatory decreasing behavior. As a result of time reversal invariance (in the case of Hermitian potentials) and unitarity one obtains the following symmetrical properties of T matrix elements:

$$T_{L'L}^{JS}(q,p;x) = T_{LL'}^{JS}(p,q;x), \tag{21}$$

$$\mathrm{Im}T_{L'L}^{JS}(q,p;k) + \sum_{L''} k[T_{L'L''}^{JS}(q,k;k)]^* T_{L''L}^{JS}(k,p;k) = 0. \tag{22}$$

Note also the occurrence of two poles corresponding to the bound state ($J=1$) at the negative relative energy $\epsilon_1 = -(\hbar^2/m)\alpha_1^2$ ($x = i\alpha_1$) and to the antibound state ($J=0$) at the energy $\epsilon_0 = -(\hbar^2/m)\alpha_0^2$ (on the unphysical sheet $x = -i\alpha_0$). The residues of the $T_{L'L}^{11}$ or T_{00}^{00} amplitudes at the poles are directly related to the Fourier transform of the deuteron or antibound state wave functions.

Now we shall again turn our attention to Eq. (12). It defines, in the momentum representation, the nonantisymmetrized elements $T_{\sigma'\sigma}^{S}(\vec{q},\vec{p};x)$. The antisymmetrized $T_{\sigma'\sigma}^{ST}(\vec{q},\vec{p};x)$ amplitudes, where T is the total isospin, are constructed with Eq. (12), but the summations over the quantum numbers JLL' satisfy the selection rule

$$(-1)^T = (-1)^{L+S+1}. \tag{23}$$

B. Numerical method

The Eqs. (14) and (15) yield a two-point boundary value problem of the type

$$Y''(r) + g(r)Y(r) = h(r). \tag{24}$$

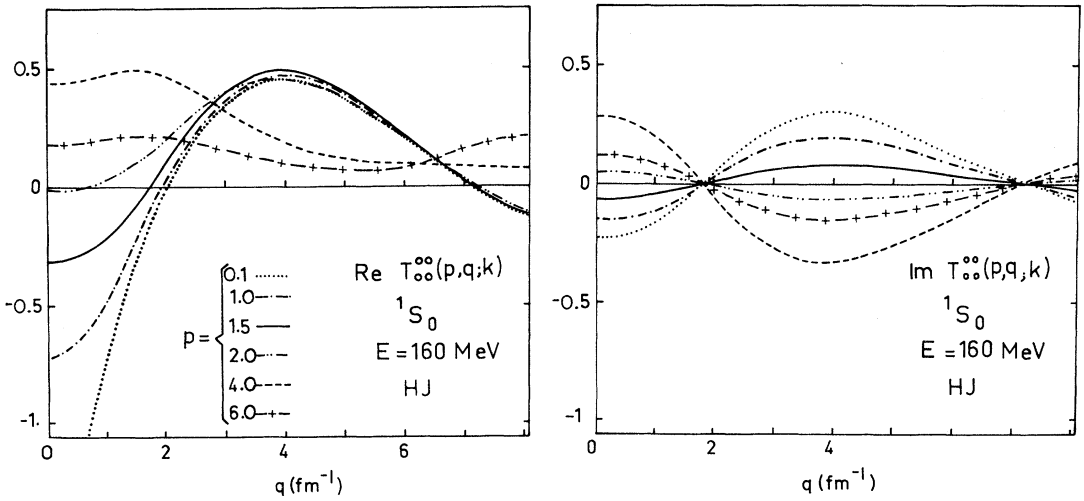

FIG. 12. $^1S_0$ fully off-shell $T_{00}^{00}(p,q;k)$ for (HJ) potential at 160 MeV. The curves are plotted against q momentum for the following p values: 0.1 (...), 1 (—·—), 1.5 (—), 2 (—···—), 4 (— — —), 6 (— + — +) fm^{-1}. Note the bundle form of the imaginary part with two nodes for $q \simeq 2$ fm^{-1} and 7 fm^{-1} which denotes the separability in p and q. The more or less separable nature of the imaginary part is diminished with increasing momenta.

In our case the functions Y, g, and h label the complex matrices

$$y^{JS}_{L'L}(r) = pr[\delta_{L'L} j_L(pr) - U^{JS}_{L'L}(r|p;x)], \quad (25)$$

$$g^{JS}_{L'L}(r) = -\left\{ \frac{m}{\hbar^2} V^{JS}_{L'L}(r) + \delta_{L'L}\left[\frac{L'(L'+1)}{r^2} - x^2 \right] \right\}, \quad (26)$$

$$h^{JS}_{L'L}(r) = -\frac{m}{\hbar^2} V^{JS}_{L'L}(r) pr j_L(pr), \quad (27)$$

which must satisfy the boundary conditions

$$y^{JS}_{L'L}(r) \to p(-i)^{L'} T^{JS}_{L'L}(x,p;x) e^{ixr} \text{ for large } r \text{ and}$$
$$U^{JS}_{L'L}(r) = 0 \text{ for } r \le r_c. \quad (28)$$

This problem is conveniently solved by the method of Ridley.[22] In this method, auxiliary complex functions s and v are introduced so that Eq. (24) is factorized in three first order equations:

$$s' - s^2 = g, \quad (29)$$

$$v' - sv = h, \quad (30)$$

$$y' + sy = v; \quad (31)$$

asymptotically, the boundary conditions are:

$$s(r) \to -ix \text{ and } v(r) \to 0 \text{ for large } r. \quad (32)$$

We prefer this complex solution to $s = x \tan xr$ used by Srivastava and Sprung which is not bounded and must be computed very carefully. Using the initial values (32) at $r = R$, Eqs. (29) and (30) are integrated inwards to kr_c, constructing punctual solutions of s and v by the Gill-Runge-Kutta method.[23] Then using $y(r_c)$ as the initial value, Eq. (31) is integrated backwards to kR, completing the solution.

In practice, during the inward calculation the functions s and v may have too rapid variations. In this case, when $\det s \neq 0$ and $|\mathrm{tr} s| \geq 10^2 k$, we switch over to the Ridley alternative method where one uses the new functions

$$S = s^{-1}$$
$$V = Sv \quad (33)$$
$$y = SY + V,$$

which satisfy the system of equations

$$S' + SgS = -1,$$
$$V' + SgV = Sh, \quad (34)$$
$$Y' - SgY = gV - h.$$

We choose a quadratic mesh with 150 points in the range (kr_c, kR) favoring the smaller r values where potentials are rapidly varying. The quadrature (17) is performed during the outward calculation. Our code calculates the $T^{JS}_{L'L}(q,p;x)$ matrix elements. Then it couples them with the $D^{JS}_{L'\sigma' L\sigma}(\hat{q},\hat{p})$ functions in order to build the antisymmetrized elements $T^{ST}_{\sigma'\sigma}(\vec{q},\vec{p};x)$. In relative values the precision is estimated to be 10^{-6} for a partial wave amplitude and 10^{-3} for $T^{ST}_{\sigma'\sigma}(\vec{q},\vec{p};x)$.

III. RESULTS FOR THE ENERGY SHELL, ITS CONTINUATION AT NEGATIVE ENERGY, AND THE BOUND STATE

A. Potentials considered

We study six potentials, assuming they are on the whole typical of the classes of "realistic potentials," i.e., of the phenomenological potentials which fit the two-nucleon observables. The Hamada-Johnston (HJ)[8,9] and Reid hard core (RHC)[5] interactions provide two types of hard core potentials. Both reproduce asymptotically the one-pion exchange potential (OPEP). The soft core potentials we retain are the soft Reid's potential (RSC),[5]

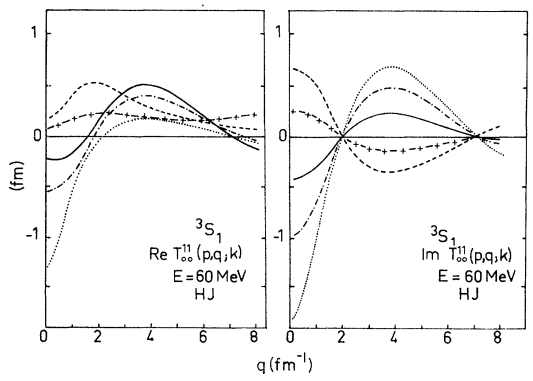

FIG. 13. $^3S_1$ fully off-shell $T^{11}_{00}(p,q;k)$ for (HJ) potential at $E = 60$ MeV. The curves are plotted against q momentum with conventions of Fig. 11. $\mathrm{Im}T^{11}_{00}$ has an apparent separability because of the weakness of the coupling with the $^3D_1$ state.

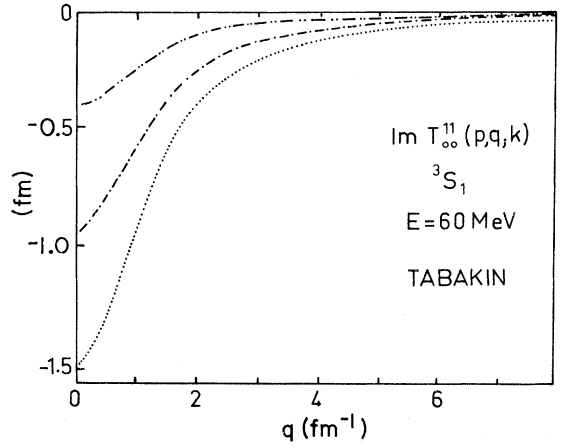

FIG. 14. $^3S_1$ fully off-shell $\mathrm{Im}T^{11}_{00}(p,q;k)$ for Tabakin's potential at $E = 60$ MeV, with the conventions of Fig. 12.

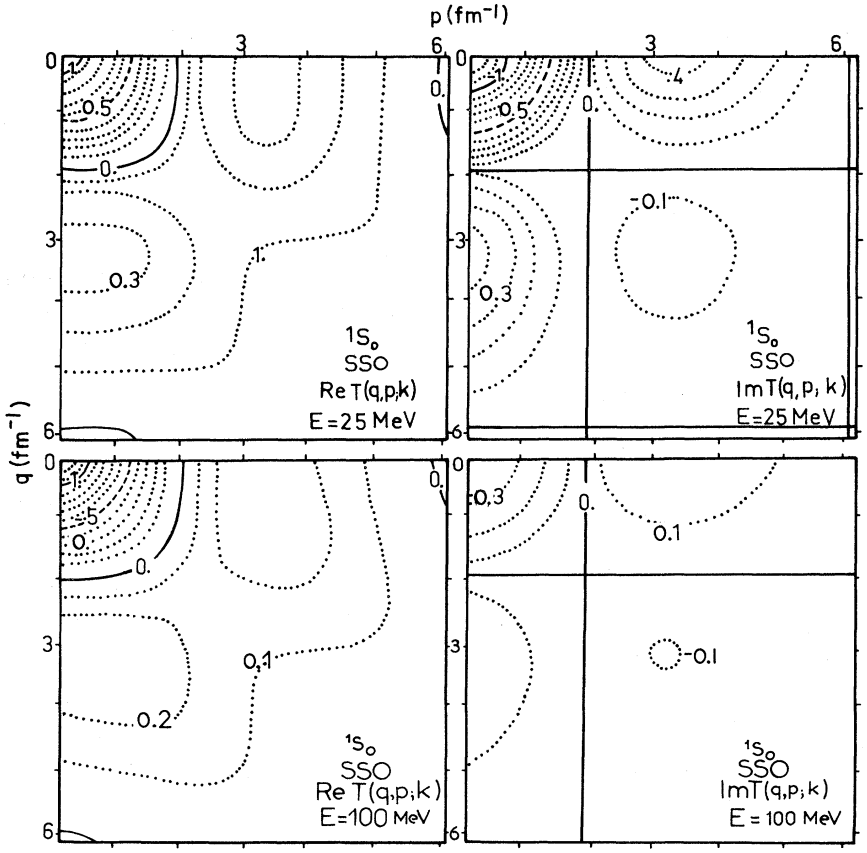

FIG. 15. $^1S_0$ fully off-shell isoamplitudes at $E=25$ and 100 MeV for (SSO) potential. Separability of the imaginary part implies that the zero level curves are straight lines parallel to the p and q axes.

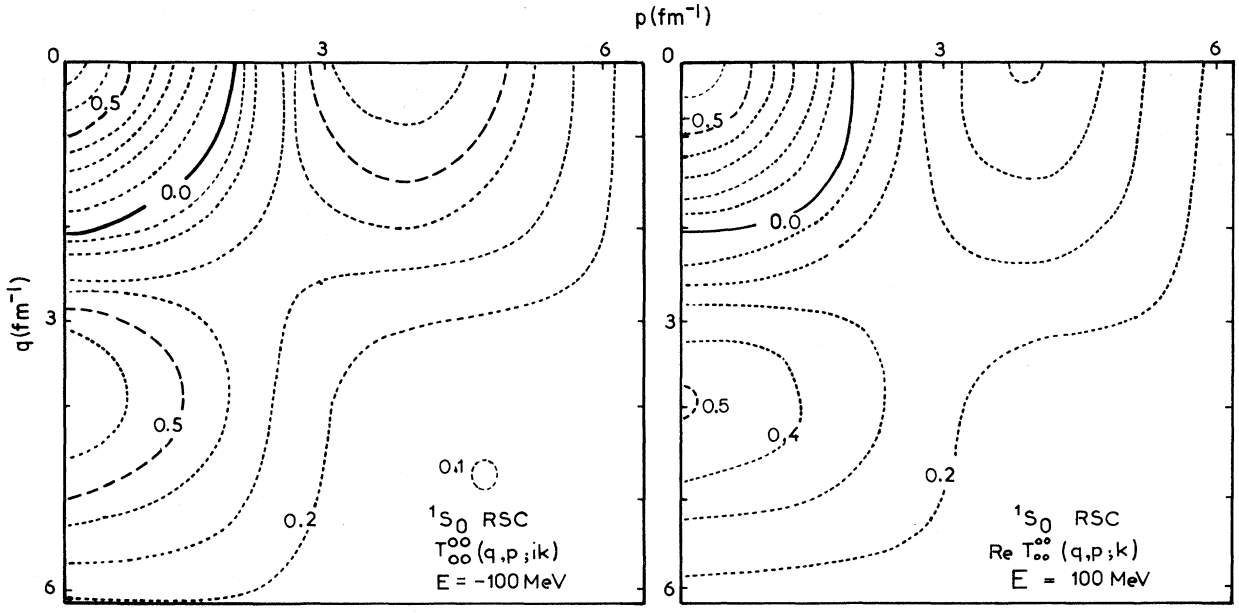

FIG. 16. Re $T_{00}^{00}(q,p;x)$ isoamplitudes at $E=-100$ MeV and +100 MeV for the (RSC) potential.

one from de Tourreil-Sprung (SSA),[7] or a preliminary version available in 1971 (SSO)[24] both containing the OPEP and a smooth potential from Gogny-Pires-de Tourreil (G1)[6] built on radial Gaussian functions.

These five potentials are local. We shall compare their behaviors with that of Tabakin's separable potential (TA)[10] which reproduces the main features of the N-N scattering data up to a relatively high energy (although it gives a bad fit to the bound state[25]).

B. Energy shell

At first we remark that the potentials quoted above are not strictly equivalent in interpreting two-nucleon scattering data. This is illustrated in Fig. 1 which gives p-n differential cross sections at four laboratory energies between 40 and 320 MeV.

In Fig. 2 the $^1S_0$ phase shift is represented as a function of k between 0 and 7 fm^{-1}. For $k<1.8$ fm^{-1} the scale chosen for the drawing does not allow one to distinguish between the local potentials. But, for $k>2$ fm^{-1}, which is out of the domain of the data used to build the potentials, the results exhibit large variations. When $k\to\infty$, (HJ) and (RHC) phase shifts go to $-kr_c$, while the soft core potentials phase shifts go to zero. In view of the results, the Tabakin potential can be classified as a super soft core interaction.

One finds similar behavior for other partial waves and for the coupling parameters ϵ_J with, however, somewhat broader deviations between the potentials in the range $k<2$ fm^{-1} than for $L=0$. The partial waves $L>0$ are mainly responsible for the spreading observed in Fig. 1.

These results exhibit the fact that the selected realistic potentials are by no means "on-shell equivalent," the main discrepancies coming from their short range behavior.

C. $p=q=k$ shell at negative energy

As an example, Fig. 3 gives $T^{00}_{00}(k,k;ik)$. The curves lie upon one another according to the order of decreasing softness of the interaction. They are constrained to fit the scattering length a_0 in the limit $E\to 0$. The spreading grows with E in the studied domain.

D. Deuteron wave function

The fitting of the deuteron observables varies somewhat among the potentials. One obtains results between -2.1 MeV (G1) and -2.5 MeV(TA) for the binding energy, and between 4% (G1) and 7% (HJ) for the D state percentage. In Fig. 4 are drawn $u(p)$ and $w(p)$, the S and D components of the deuteron wave function in momentum space calculated with the (HJ) and (SSO) potentials. The main discrepancies come from their different D state percentages. The other local potentials give very similar results. The phenomenological S-wave functions from Hulthen and Sugawara[26] and Moravcsik[27] are drawn for the sake of comparison.

IV. GENERAL FEATURES OF OFF-SHELL AMPLITUDES

The transition operator $T(\vec{q},\vec{p};x)$ is a complex function of the variables $\vec{q},\vec{p}$ and x. To understand the general features of its off-shell matrix ele-

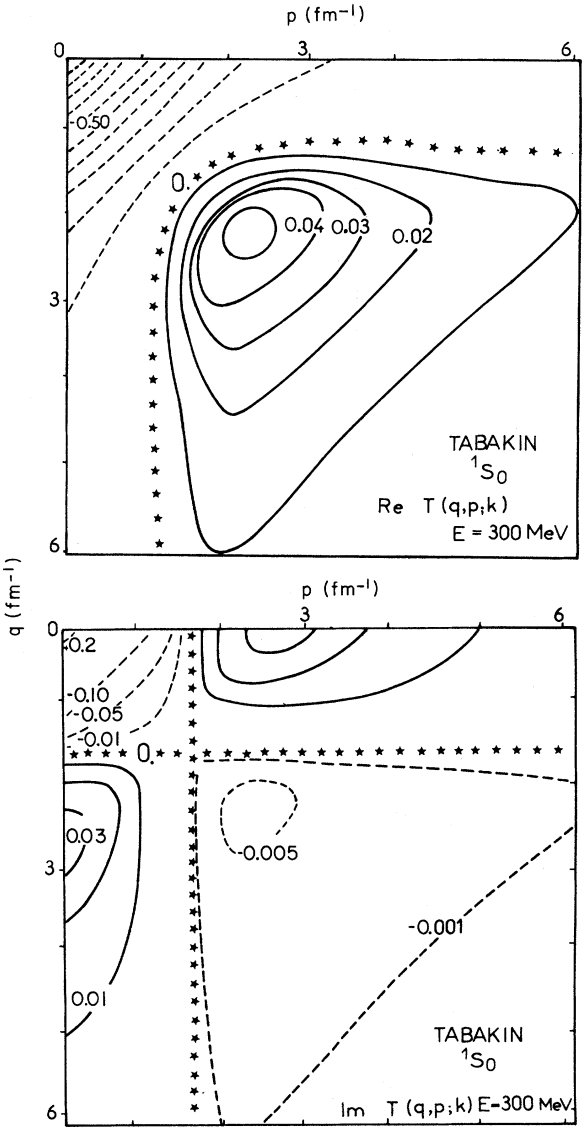

FIG. 17. $^1S_0$ fully off-shell isoamplitudes at $E=300$ MeV for the (TA) potential.

ments and especially their behavior in energy and momentum, we shall give some selected results for values of p and q up to 8 fm^{-1}. Though the domain of validity of a potential description of N-N interaction limits the momenta up to 2 fm^{-1} ($E_{\text{lab}} \sim 320$ MeV), we have to consider in nuclear theories off-the-energy-shell amplitudes as mathematical functions which are integrated over large momenta.

We shall explore off-shell amplitudes for p and q values only up to 8 fm^{-1}, since in nuclear theories the contributions of the higher momenta are always weighted by wave functions whose significant values occur only in a range of a few fm^{-1}. We computed the $T^{JS}_{L'L}(p,q;x)$ amplitudes up to $J=6$ for the set of potentials: RHC, RSC, HJ, G1, and SSO.

In Fig. 5, we show the $^1S_0$ amplitude at positive energy $e^{-i\delta_0(k)}T^{00}_{00}(q,k;k)$ for $k=1.5$ fm^{-1}. The pinching of the curves near $q=k$ exhibits the on-shell constraints. On both sides their discrepancies reflect the different degrees of hardness of the potential cores. At negative energy, the discrepancies are enhanced because of the lack of on-shell constraints. See in Fig. 6 the $^3S_1$ state Re $T^{11}_{00}(q,k;k)$. Near $E \sim 20$ MeV, the phase shift crosses $\frac{1}{2}\pi$; then $T^{11}_{00}(k,k;k)$ goes to zero. This property is extended to the half-off-shell amplitudes by the unitarity relation.

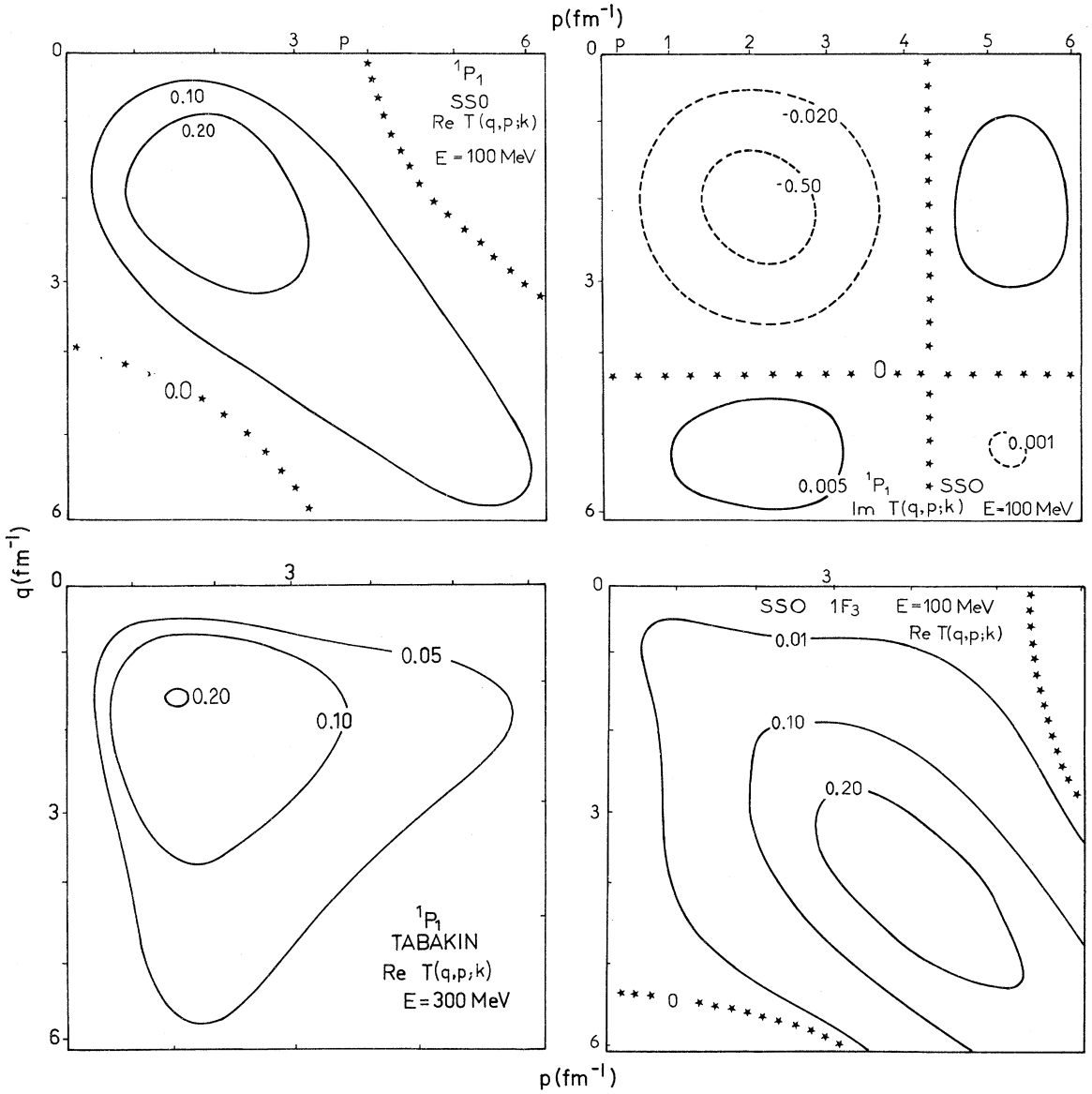

FIG. 18. $^1P_1$ and $^1F_3$ isoamplitudes for (SSO) and (TA) potentials.

In Fig. 7 we give the $^1S_0$ half-shell isoamplitudes $e^{-i\delta_0^0(k)}T_{00}^{00}(q,k;k)$ in the $\{q,k\}$ plane. To understand their topological features, we calculate the $^1S_0$ half-off-shell amplitudes for a square well potential, with range $a=2.54$ fm and depth 14.5 MeV, which fits the low energy parameters (Fig. 8). For lower momenta ($p,q<2$ fm^{-1}) the deep hole of the realistic local potentials is well reproduced; outside one observes a smooth diffraction structure parallel to the diagonal with a period $\Delta q=\Delta k\simeq\pi/2a$. If we add a hard core barrier with radius $r_c=0.5$ fm, the resulting potential model gives a topology (Fig. 9) very similar to that of (HJ) or (RHC) potentials. With a pure hard sphere potential [Eq. (19)], one gets parallel straight lines with dampened oscillations and a pseudoperiod $\Delta p=\Delta q=\pi/2r_c$. Thus the behavior of the amplitudes for high k or q values are explained by a hard sphere scattering. The hump near $q=4$ fm^{-1} is due to the short range repulsion of local potentials. Its width and its height increase with the hardening of the potentials. The two-rank separable interaction (TA) is less picturesque because of the diffuseness induced by the nonlocality.

As regards the $^1P_1$ state, Fig. 10 shows that the core influence is still discernible; in the (HJ) case we again find the asymptotic characteristic lines parallel to the k axis. The different structures of the isocurves (HJ) and (SSO) are well understood from the $^1P_1$ phase shift properties which determine the values of the isocurves on the diagonal. For $k>2$ fm^{-1} the potentials get phase shifts analogous to those of the $^1S_0$ case. However, $e^{-i\delta_1^1}\times T_{11}^{10}(k,k;k)$ must vanish for $k=0$ while, in the $^1S_0$ state, it is equal to the negative scattering length a_0, giving rise to the characteristic deep hole. In Fig. 11 we give an example of half-off-shell isocurves for the $^1D_2$ state.

For the fully off-shell $T_{L'L}^{JS}(q,p;x)$ calculated at fixed positive or negative energies, we give some typical curves in Figs. 12–18. In case of noncoupled states, Im $T_{LL}^{JS}(q,p;k)$ is separable (Figs. 12, 15, and 17) because of the unitarity [Eq. (22)].

The fully off-shell isoamplitudes in the $\{p,q\}$ plane outline the symmetrical properties in p and q. The quantity Re $T_{00}^{JS}(q,p;x)$ is weakly energy dependent in the range $E=25$–300 MeV (Figs. 15 and 16), while Im $T_{00}^{JS}(q,p;k)$ is nearly proportion-

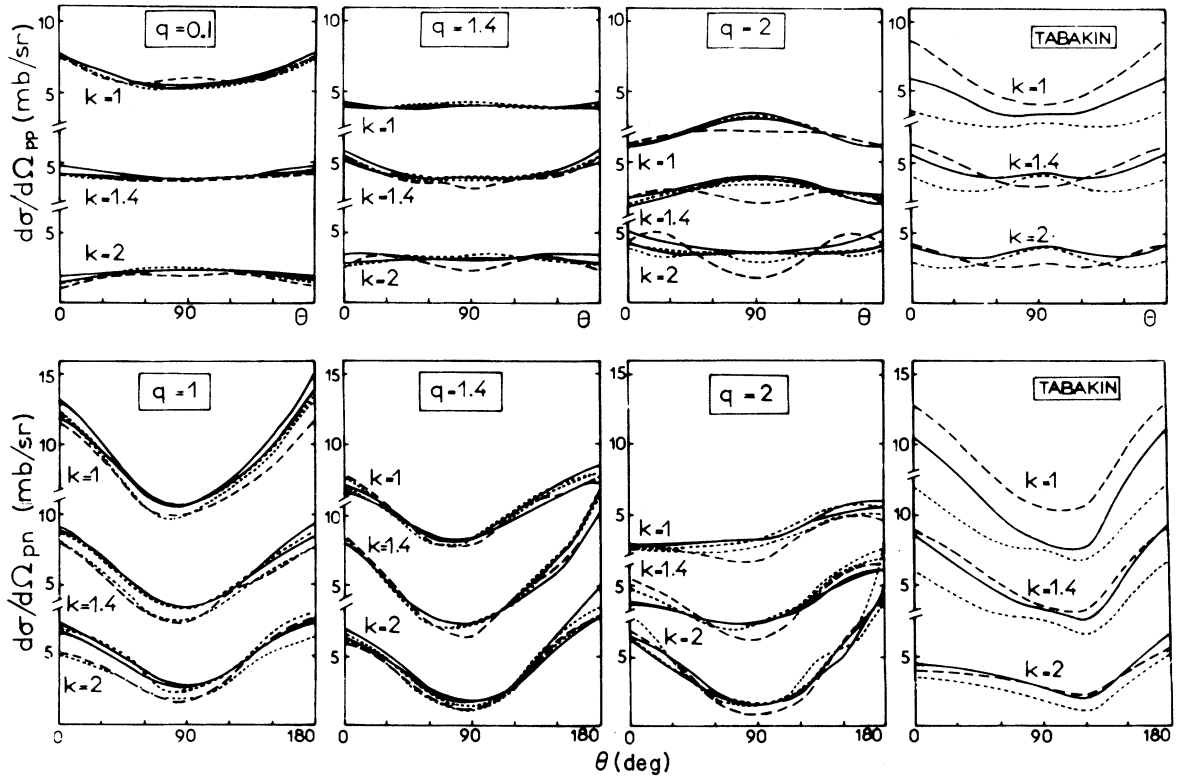

FIG. 19. Half-shell cross sections $d\sigma_{pp}(\vec{q},\vec{k};k)/d\Omega$ and $d\sigma_{pn}(\vec{q},\vec{k};k)/d\Omega$ for $k=1$, 1.4, and 2 fm^{-1} ($E=80$, 160, and 320 MeV) as functions of the angle θ between $\vec{k}$ and $\vec{q}$. The first three columns correspond to (HJ) and (RHC) (—), (RSC) and (SSO) (...) and (G1) (– – –) potentials with q values of 1, 1.4, and 2 fm^{-1}, respectively. The fourth column collects the same results for Tabakin's potential for $q=1$ (– – –), $q=1.4$ (—), and $q=2$ (...) fm^{-1}. The p-p cross sections do not include the Coulomb interaction.

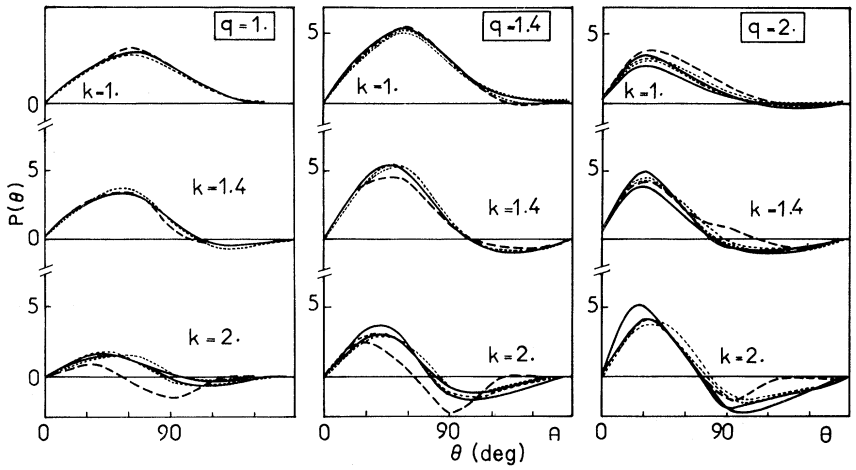

FIG. 20. Half-shell p-n polarizations for the local potentials. Conventions are given in the caption of Fig. 19.

al to E, see Fig. 15. For highest L states, the interaction takes place peripherally so that the amplitudes are practically the momentum representation of the long range part of the potential. As a consequence, if V is local, the diagonal $p=q$ looks like a ridge line of the level curves.

V. OFF-SHELL CROSS SECTIONS AND ON-SHELL APPROXIMATIONS

A. Off-shell cross sections and polarizations

Off-shell cross sections are calculated from the antisymmetrized operators $T^T(\vec{q},\vec{p};x)$ defined by Eq. (23),

$$\frac{d\sigma}{d\Omega_{pp}}(\vec{q},\vec{p};x)=\pi^4 m^2\,\mathrm{tr}[T^{1+}(\vec{q},\vec{p};x)T^1(\vec{q},\vec{p};x)]\ , \tag{35}$$

as functions of θ, the angle between $\vec{p}$ and $\vec{q}$, at the positive or negative energy $E=2(\hbar^2/m)x^2$. The cross section $d\sigma/d\Omega_{pn}$ is calculated in the same way but with $\frac{1}{2}(T^0+T^1)$ instead of T^1. Off-shell polarizations are computed similarly. These quantities give a global estimation of off-shell effects and available variations between the potentials. For momenta p, q, and k, we use three

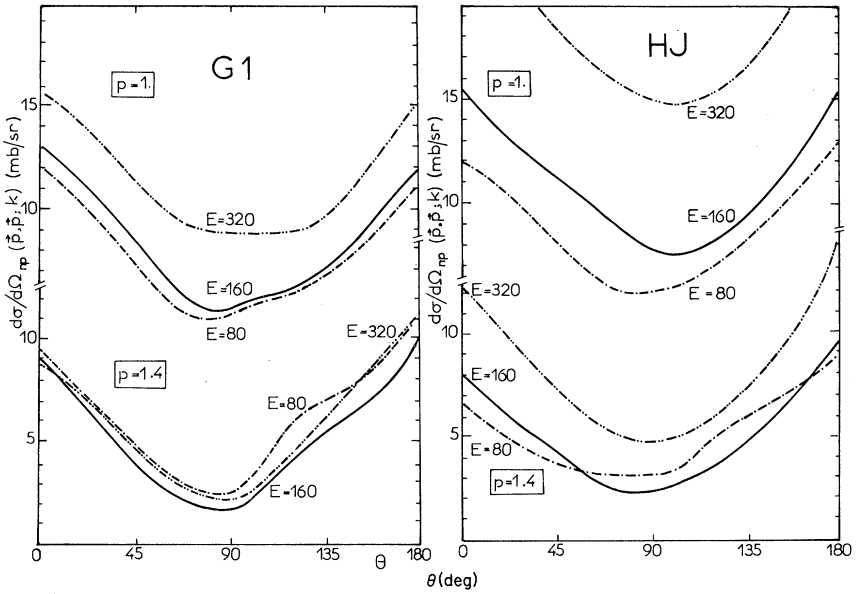

FIG. 21. Fully off-shell "diagonal" cross sections $d\sigma_{np}(\vec{p},\vec{p};k)/d\Omega$ for $E=80$ (—·—), 160 (—), and 320 (—···—) MeV, $p=1$ and 1.4 fm^{-1} calculated with (G1) and (HJ) potentials.

values 0.98, 1.39, and 1.96 fm^{-1}, which correspond to 80, 160, and 320 MeV laboratory energies.

Results for the half-shell $d\sigma(\vec{q}, \vec{k}; k)/d\Omega$ are drawn in Fig. 19 for the pn and pp cases (the Coulomb field is omitted) and in Fig. 20 for the pn half-shell polarization. One notes that the spreading between the local potentials has the same magnitude off and on the energy shell ($k = q$). At very low energy, the discrepancies between the potentials increase. For instance, at $E = 1$ MeV and $q = 2$ fm^{-1}, one obtains for the p-n case ratios up to 10. For this reason, the off-shell effects may play a nonnegligible role in a nuclear reaction with a kinematic of final state interaction. Tabakin's shapes are clearly different especially at backward angles, but this potential affects too few partial waves ($L \leq 3$).

Studying the negative energy cross sections $d\sigma(\vec{q}, \vec{k}; ik)/d\Omega$, we observed larger deviations between the potentials, as one might have expected from the analysis of the partial wave results (Fig. 3).

For the "diagonal" elements $d\sigma(\vec{p}, \vec{p}; x)/d\Omega$ the soft potential (G1) looks like (SSO) while the hard one (RHC) is similar to (HJ). In Fig. 21, we give the results obtained for (G1) and (HJ) at positive energies. Note that the cross sections are more sensitive to p than to E.

Compared to $d\Omega(\vec{p}, \vec{p}; x)/d\Omega$ the fully off-shell $d\sigma(\vec{p}, \vec{q}; x)/d\Omega$ for given p and x seem to be smaller.

B. On-shell approximations

Several on-shell approximations for the off-shell two-nucleon T matrix have been used in the impulse approximation description of elastic and inelastic nucleon-nucleus scattering and $(p, 2p)$ reaction. They relate a $T(\vec{q}, \vec{p}; x)$ to an on-shell amplitude $T(\hat{\vec{k}}', \hat{\vec{k}}; \hat{k})$ at suitable energy $\hat{E} = 2(\hbar^2/m)\hat{k}^2$ and angle $\hat{\theta}$ between $\hat{\vec{k}}$ and $\hat{\vec{k}}'$.

Stephenson *et al.*[20] have studied the quality of on-shell prescriptions for $(p, 2p)$ reactions on very heavy nuclei, the knocked-out proton being bound by 45 MeV. We come back to this problem, but for the scattering on a deuteron (i.e., a nucleus of small binding energy $\epsilon_1 = -(\hbar^2/m)\alpha_1^2 \approx -2.22$ MeV) of a proton with laboratory energy

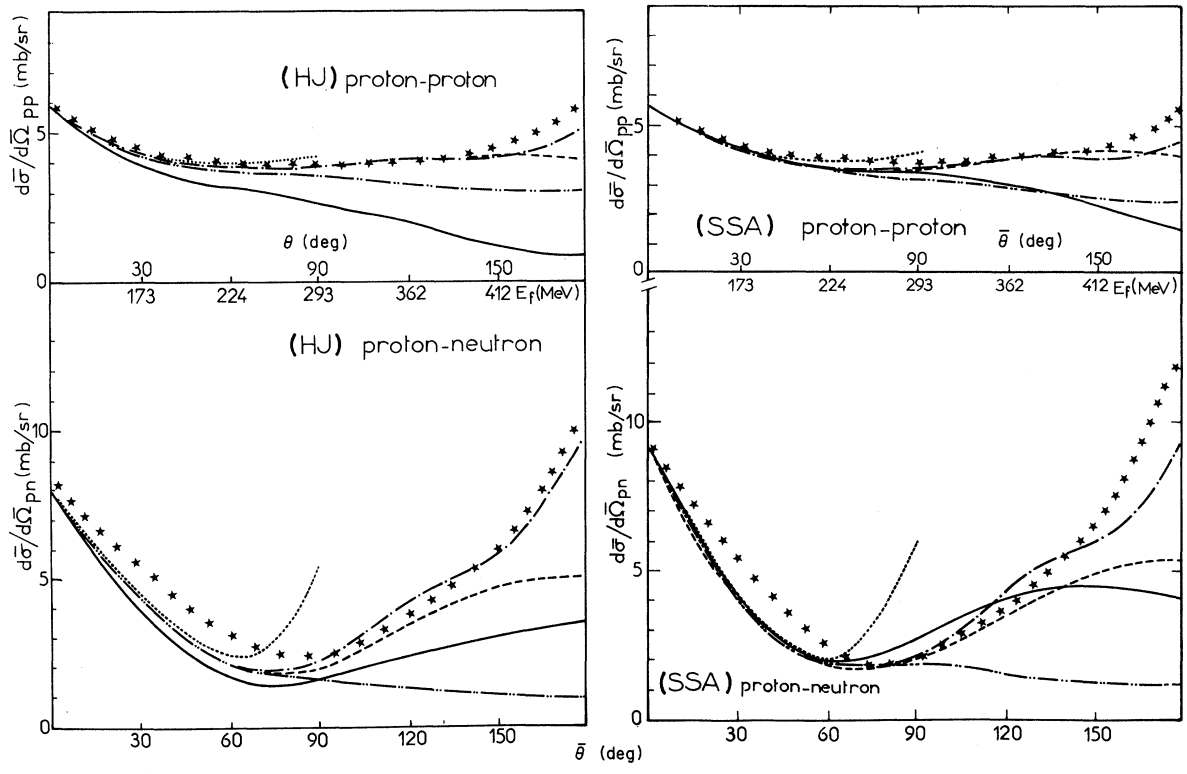

FIG. 22. Off-shell p-p and p-n cross sections relevant to the impulse approximation of $d(p,p)d$ scattering at $E_0 = 155$ MeV for (SSA) and (HJ) potentials (in full lines). Corresponding on-shell approximations as defined in the text: (OEI) (★★★), $\hat{E} = E_0$ (. . .), $\hat{E} = E_f$ (— · · —), $\hat{E} = \frac{1}{2}(E_0 + E_f)$ (— — —), and $\hat{E} = \frac{1}{16}(9E_0 + 7E_f)$ (— • —). On the abscissa are given the values of $\bar{\theta}$ (three-body c.m. angle) and E_f.

$E_0 = 2(\hbar^2/m)k_0^2$.

In the impulse approximation treatment of the elastic $d(p,p)d$ scattering, when the two-body matrix is factorized for zero momentum of the struck nucleon, the amplitude is a function of the off-shell matrix element $T(\vec{q},\vec{p};x)$ with momenta $\vec{q} = \vec{k}_0 - \vec{K}$, $\vec{p} = \vec{k}_0$, $x = (k_0^2 - \alpha_1^2)^{1/2}$ and energies $E_f = 2(\hbar^2/m)q^2$, $E_i = 2(\hbar^2/m)p^2 = E_0$, where $2\vec{k}_0$ is the initial momentum of the incident nucleon in the laboratory and K is the transfer momentum in the scattering on the nucleus.

The shell deviation is $\Delta E = E_f - E_i = (\hbar^2/2m)K^2$, ΔE increases with K from 0 to $\frac{16}{9}E_0$. As an example, the two-nucleon off-shell cross sections at $E_0 = 155$ MeV, corresponding to (HJ) and (SSA) potentials, are plotted in Fig. 22 against $\bar{\theta}$, the center of mass scattering angle of the $p+d$ system. As ϵ_1 is negligible compared with E_0, the cross sections are nearly half-shell at the initial energy. The discrepancies between the potentials can reach 10% even near the on-shell point $\bar{\theta} = 0°$. In Fig. 22 we compare five on-shell approximations to these off-shell cross sections. In the so-called "on-energy-shell impulse approximation" (OEI), one takes $\hat{k} = k_0$ and $\hat{\theta} = \bar{\theta}$. This prescription does not preserve the transfer momentum, which becomes $\frac{3}{4}\vec{K}$. In the four other approximations, one maintains the length of $\vec{K}$ which gives $\hat{\theta} = 2\arcsin\frac{1}{2}K/\hat{k}$ and for $\hat{E}$ one takes E_0, E_f, $\frac{1}{2}(E_0+E_f)$, or[28] $\frac{1}{16}(9E_0+7E_f)$.

Except for (OEI), the discrepancies between the on-shell approximations and corresponding exact

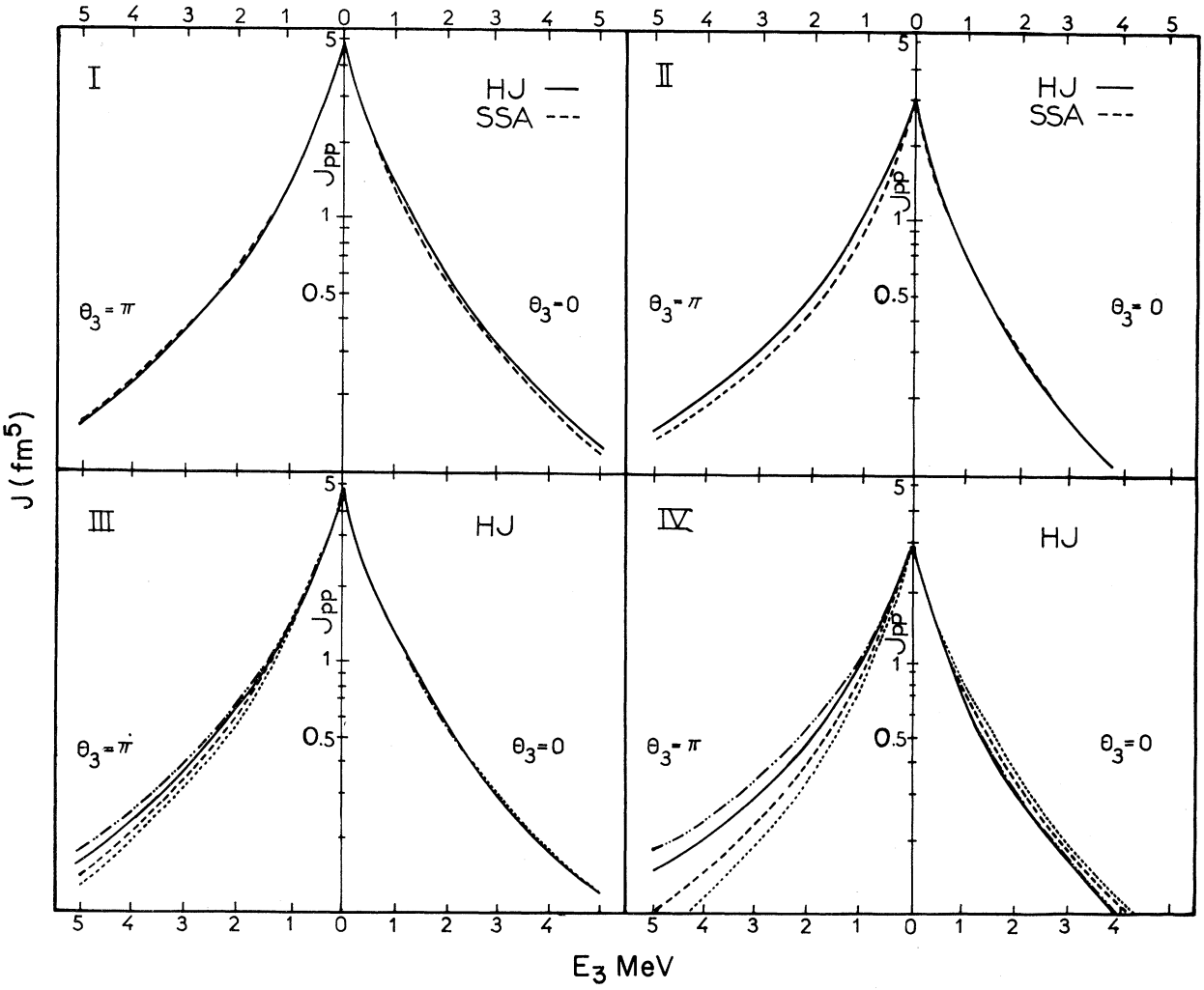

FIG. 23. The functions J_{pp} and J_{pn} relevant to p-d breakup in the nucleon spectator model [see Eq. (36)] and with symmetric geometry are shown as a function of the spectator nucleon energy E_3 for $E_0 = 155$ MeV. We compare the off-shell calculations with (HJ) (–) and (SSA) (– – –) in parts I and II. For (HJ) interaction corresponding on-shell approximations a (. . .), b (– · · –), c (– – –), and d (– · –) defined in the text are given in Secs. III and IV.

off-shell calculation are less, for $\bar{\theta} < 60°$, than differences due to the potentials. For $\bar{\theta} > 60°$ these approximations are clearly less good, but in this region the factorized impulse approximation is known not to reproduce the experimental data.

The impulse approximation amplitude of the $d(p, 2p)n$ reaction is a function of the half-shell matrix elements $T(\vec{k}, \vec{p}; k)$. Let $\vec{p}_1$, $\vec{p}_2$, and $\vec{p}_3$ be, respectively, the final momenta of the two protons and neutron in the laboratory system, and E_3 the neutron energy. We consider the kinematical region $E_3 \ll E_0$, where the impulse approximation is supposed to be valid (spectator neutron approximation). One has $\vec{k} = \frac{1}{2}(\vec{p}_1 - \vec{p}_2)$, $\vec{p} = \vec{k}_0 + \frac{1}{2}\vec{p}_3$. The shell deviation is $\Delta E = 2E_3 - \epsilon_1$. Having removed the kinematical factor, the cross section is expressed by

$$J_{PP} = \frac{1}{4\pi}[u^2(p_3) + w^2(p_3)]\frac{d\sigma}{d\Omega_{pp}}(\vec{k}, \vec{p}; k) \ . \qquad (36)$$

As an example we consider a symmetrical geometry: $E = E_f = 2(\hbar^2/m)k^2$ is larger (smaller) than E_0 when the neutron is emitted forwards (backwards). The quantity J_{pp} calculated for (HJ) and (SSA) potentials at $E_0 = 155$ MeV is plotted in Fig. 23 against $E_3 \leq 5$ MeV. The analogous J_{pn} corresponding to the $d(p, pn)p$ reaction are also shown in the same figure.

In the symmetrical geometry $\vec{p} \cdot \vec{k} = 0$, we studied three on-shell approximations defined by $\hat{\theta} = 90°$ and $\hat{E} = E_0, E_f, \frac{1}{2}(E_0 + E_f)$ (labeled respectively a, b, and c in Fig. 23). We considered a fourth one (d) which preserves the two-body transfer $\vec{K} = \vec{p} - \vec{k}$ by introducing an auxiliary vector $\vec{Q}$ parallel to $\vec{K}$, such as $\hat{\vec{k}}' = \vec{p} + \vec{Q}$, $\hat{\vec{k}} = \vec{k} + \vec{Q}$, with $\hat{k} = \hat{k}'$.

The approximations are very good when the spectator nucleon is emitted forward, especially in the p-p case. The best fit is obtained with the fourth approximation.

VI. CONCLUSION

We have developed a practical method of calculating the fully off-shell T matrix elements for any partial wave using local N-N potentials with soft or hard cores. The work supplements the previous work of Srivastava and Sprung.

We have compared the results obtained with five realistic local potentials and the Tabakin separable potential. Since these potentials are not phase-shift equivalent, the on-shell T matrix elements display large differences for $k > 2$ fm^{-1}, related to the short range behavior of the potentials. There are similar differences in the off-shell results.

We have shown that the square well potentials with repulsive cores which contain the general trends of the local realistic potentials reproduce the gross features of the off-shell T matrix elements. The scattering amplitudes $T^{JS}_{L'L}(p, q; k)$ arise from the interference between two parts. The first, corresponding to the long range part of the force, dominates whenever p, q, and k are small; when p and q are large it gradually decreases as a diffractive picture when one goes far from the $p = q$ shell. The second part originates in the potential core region; it looks like a hard sphere amplitude and has a diffractive behavior in the p and q directions with a pseudoperiod inversely proportional to the effective core radius; its magnitude is directly related to the strength of the repulsive core.

In itself, the present analysis does not allow one to foresee the ability of many-body calculations to select among the different two-nucleon potentials, since this ability depends mainly on the off-shell sensitivity of the studied problem. Furthermore, up to now, most of the many-body problems have been solved in the framework of models and approximations whose accuracy is not well known. It will, then, be difficult to draw any conclusions when the off-energy-shell deviations between the potentials are small.

---

*Laboratoire Associé au Centre National de la Recherche Scientifique.

[1]M. M. MacGregor, R. A. Arndt, and R. M. Wright, Phys. Rev. 169, 1128 (1968); 173, 1272 (1968); 182, 1715 (1969); R. A. Arndt, R. H. Hackman, and L. D. Roper Phys. Rev. C 9, 555 (1974).

[2]G. Breit and R. D. Haracz, in *High Energy Physics* edited by E. M. S. Burhop (Academic, New York, 1967), Vol. 1, p. 21.

[3]C. N. Bressel, A. K. Kerman, and B. Rouben, Nucl. Phys. A124, 624 (1968).

[4]E. L. Lomon and H. Feschbach, Ann. Phys. (N.Y.) 48, 94 (1968).

[5]R. V. Reid, Jr., Ann. Phys. (N.Y.) 50, 411 (1968).

[6]P. Pires (private communication); P. Pires, thèse de doctorat d'Etat, Université Paris XI, 1973 (unpublished); D. Gogny, P. Pires, and R. de Tourreil, Phys. Lett. 32B, 591 (1970).

[7]R. de Tourreil and D. W. L. Sprung, Nucl. Phys. A201, 193 (1973).

[8]T. Hamada and I. D. Johnston, Nucl. Phys. 34, 382 (1962).

[9]T. Hamada, Y. Nakamura, and R. Tamagaki, Prog. Theor. Phys. 33, 769 (1965).

[10]F. Tabakin, Ann. Phys. (N.Y.) 30, 51 (1964).

[11]F. Tabakin and K. T. R. Davies, Phys. Rev. 150, 793

(1966).
[12]F. Tabakin, Phys. Rev. 174, 1208 (1968).
[13]T. R. Mongan, Phys. Rev. 175, 1260 (1968); 178, 1597 (1969); Lawrence Radiation Laboratory University of California Report No. 18630, 1968 (unpublished); Phys. Rev. 180, 1514 (1969).
[14]D. D. Brayshaw, Phys. Rev. C 7, 1731 (1973).
[15]M. K. Srivastava and D. W. L. Sprung, Nucl. Phys. A139, 605 (1969); A149, 113 (1970).
[16]D. W. L. Sprung, in *Proceedings of the International School of Elementary Particle Physics at Herceg-Novi, Yugoslavia, 1970* (Secretariat du Departement de Physique Corpusculaire, Centre de Recherche Nucléaires, Strasbourg-Cronenberg, France, 1970).
[17]M. K. Srivastava, Nucl. Phys. A157, 61 (1970); 221, 183 (1974).
[18]T. Takemiya, Prog. Theor. Phys. 48, 1547 (1972); 49, 1602 (1973).
[19]I. McCarthy and P. C. Tandy, Nucl. Phys. A178, 1 (1971).
[20]G. J. Stephenson, Jr., E. F. Redish, G. M. Lerner, and M. I. Haftel, Technical Report No. 73-002, University of Maryland Department of Physics and Astronomy, College Park, Maryland (unpublished).
[21]M. L'Huillier, thèse de doctorat d'Etat, Université Paris VII, 1974 (unpublished).
[22]E. C. Ridley, Proc. Camb. Philos. Soc. 53, 442 (1957).
[23]S. Gill, Proc. Camb. Philos. Soc. 47, 96 (1951).
[24]R. de Tourreil and D. W. L. Sprung (private communication).
[25]The numerical code to handle Tabakin interaction has been worked out with M. Morlet, B. Tatischeff, and A. Willis.
[26]L. Hülthen and M. Sugawara, Handb. Phys. 39, 74 (1957).
[27]M. J. Moravcsik, Nulc. Phys. 7, 113 (1958).
[28]K. L. Kowalski and D. Feldman, Phys. Rev. 130, 276 (1973).